Heliyon 7 (2021) e08585

Contents lists available at ScienceDirect

Heliyon

journal homepage: www.cell.com/heliyon

Research article

Pressure dependent structural, elastic and mechanical properties with ground state electronic and optical properties of half-metallic Heusler compounds Cr_2YAl (Y=Mn, Co): first-principles study

M. Jubair [a,*], A.M.M. Tanveer Karim [a], M. Nuruzzaman [a], M. Roknuzzaman [b], M.A.K. Zilani [a]

[a] Department of Physics, Rajshahi University of Engineering and Technology, Rajshahi, 6204, Bangladesh
[b] Department of Physics, Jashore University of Science and Technology, Jashore, 7408, Bangladesh

ARTICLE INFO

Keywords:
Heusler compound
First-principles calculations
Elastic constants
Electronic properties
Half-metal

ABSTRACT

Hydrostatic pressure dependent structural, electronic, elastic and optical properties of Heusler compounds Cr_2YAl (Y=Mn, Co) are investigated by the first-principles calculations. Present study shows good agreement between the calculated and experimental values of lattice parameters of these compounds. The gradual decrease of lattice parameter and unit cell volume with the increase of pressure eliminates the possibility of phase transition up to the considered pressure range 0–30 GPa. The absence of negative frequency in the phonon dispersion curves at various external pressures up to 30 GPa confirm the dynamical stability of these compounds. The values of Pugh's ratio, Poisson's ratio and Cauchy pressure indicate the ductility of Cr_2CoAl while those criteria confirm the brittleness of Cr_2MnAl. Pressure dependent behaviour of the elastic constants of these compounds shows the mechanical stability over the studied pressure range (0–30 GPa). Crystal stiffening of both the compounds is indicated by the increase of Debye temperature with increasing hydrostatic pressure. The pressure dependent band structure and density of states (DOS) calculations reveal the half- and the near half-metallic behaviour of Cr_2MnAl and Cr_2CoAl, respectively up to 20 GPa while those disappears at pressure around 30 GPa. The variations of optical constants with pressure is consistent with the results of the electronic structure calculations. High reflectivity (>45%) of both the compounds makes them attractive for optoelectronic device applications.

1. Introduction

A class of intermetallic compounds known as Heusler alloys are still attractive in the current century in spite of the fact that these compounds were discovered in 1903 [1]. As there is huge interest of Heusler alloys in various fields especially in spintronics, a lot of them were studied experimentally and theoretically over the last few decades. Many of the Heusler alloys are half metallic; half metallicity indicates that these compounds are metallic for one type of spin and semiconducting for other type of spin. There are scopes to synthesize or predict new Heusler compounds and investigate their various physical properties which can make them suitable for many technological applications, e.g., spintronics [2, 3], magnetic tunnel junction [4], electrodes for giant magnetoresistive spin valves, injection of spins into semiconductors [5], magnonics [6], shape-memory materials [1], spin-torque oscillators [7, 8], magnetic memory [9] etc. Some of these materials can provide an interesting platform for novel quantum phenomena such as quantum Hall effect, quantum chromodynamics etc. [10]. Huesler alloys with superconducting properties also have been reported and attracted significant research interest [11, 12].

Heusler alloys are represented by the generic formula X_2YZ (Full Hesulers) and XYZ (Half-Hesulers) both with face-centered cubic (FCC) crystal structure, where X and Y are transition elements and Z is the group III, IV or V elements. For X_2YZ Hesuler compounds, X and Y atoms are located at positions (0,0,0), (1/4,1/4,1/4) and (1/2,1/2,1/2); Z atom is located at (3/4,3/4,3/4). There are two types of structures of X_2YZ Hesuler compounds: Cu_2MnAl-type and Hg_2CuTi-type. In Cu_2MnAl-type structure, two X atoms are located at the sites (0,0,0) and (1/2,1/2,1/2); Y atom is located at the site (1/4,1/4,1/4); Z atom is located at the site (3/4,3/4,3/4). On the other hand, in Hg_2CuTi-type structure, two X atoms are located at the sites (0,0,0) and (1/4,1/4,1/4); Y atom is located at the site (1/2,1/2,1/2); Z atom is located at the site (3/4,3/4,3/4) [13].

Jamer *et al* prepared bulk Cr_2CoAl and predicted the presence of both ferrimagnetic and paramagnetic phases [14]. Under Argon atmosphere,

* Corresponding author.
E-mail address: jubair016@gmail.com (M. Jubair).

https://doi.org/10.1016/j.heliyon.2021.e08585
Received 10 July 2021; Received in revised form 24 October 2021; Accepted 8 December 2021

polycrystalline Cr_2CoAl was synthesized by arc melting [15]. When the alloy Cr_2CoAl was cooled below 28K, the compound would be ferromagnetic. A study of effect of disorder in Cr_2CoAl shows that spin magnetic moment varies with atomic disorder [16]. *Ab initio* calculations of structural stability, magnetism, and electronic structure of Cr_2MnAl, Cr_2CoAl and some other Heusler compounds are done by various research groups [5, 14, 17, 18, 19]. There is a density functional theory (DFT) study regarding undoped and Fe-doped Cr_2CoAl [20]. This study predicted that these compounds are not true half-metallic ferromagnets. Another computational study showed that Cr_2CoAl is a compensated half-metal (CHM) [21]. There is a DFT study which confirms the half metallicity of Cr_2MnAl [22]. According to this study, the magnetic moment calculation of Cr_2MnAl is consistent with Slater-Pauling rule.

Study of optical properties can provide useful insight which is helpful to judge the adaptability of potential application in optoelectronic device construction. One recent computational study focused only on the ground state optical properties of Cr_2CoAl [19]. To the best of our knowledge, optical properties of Cr_2MnAl are not yet explored. Here we focus on the ground state as well as the pressure dependent optical properties of these compounds. The effect of pressure on lattice parameter, unit cell volume and the elastic properties are important because it can identify any structural phase change and unstable condition of the compounds. Pressure dependence of the structural, elastic and mechanical properties of the compounds Cr_2YAl (Y=Mn, Co) are studied here. The phonon dispersion curve usually helps to understand the dynamical stability of solids. The absence of imaginary frequency in dispersion curves suggests the stability of a system. The phonon dispersion curves of Cr_2MnAl and Cr_2CoAl along high symmetry directions in the Brillouin zone up to pressure 30 GPa are investigated. The Debye temperature and the acoustic velocities are also calculated because these parameters along with elastic constants are important to find their potential industrial applications. The study of the electronic properties such as band structure and DOS helps to judge the conducting nature and to explain the optical properties of a compound. Thus the effect of pressure on the ground state band structure and DOS of these compounds are also studied.

2. Computational method

DFT is a quantum theory based popular method to calculate physical properties of a solid system. Computational study of Cr_2YAl (Y=Mn, Co) are done by CAmbridge Serial Total Energy Package (CASTEP) code [23] based on DFT [24, 25]. To evaluate exchange correlation energy PBE-GGA scheme is used [26]. The electron-ion interaction is considered by Vanderbilt type ultrasoft pseudopotentials [27]. Broyden, Fletcher, Goldfrab and Shanno technique is used to optimize the structure [28]. To optimize the crystal structure and to calculate all the properties including DOS of Cr_2CoAl (Cr_2MnAl) a plane wave cut off energy of 500 eV (350 eV) and $12 \times 12 \times 12$ ($9 \times 9 \times 9$) Monkhorst-Pack grid [29] are used. Convergence threshold for total energy is taken as 1×10^{-5} eV/ atom. The calculations are done with the convergence threshold of 0.03 eV/Å for the maximum force, 0.05 GPa for maximum stress, and 0.001Å for maximum displacement. The phonon dispersion calculations are performed by using the finite displacement supercell method [30] considering a $3 \times 3 \times 3$ supercell, cut off energy of 310 eV and k point mesh of $7 \times 7 \times 7$.

3. Results and discussion

3.1. Structural properties

Both Cr_2YAl (Y=Mn, Co) possess a unit cell having FCC structure with space group $F\bar{4}3m$ (No.216). The unit cell having four formula units contains 16 atoms. The crystal structure of Cr_2YAl (Y=Mn, Co) is shown in Figure 1. In the unit cell of Cr_2YAl (Y=Mn, Co), Cr atom occupies the Wyckoff positions (0,0,0) and (1/4,1/4,1/4), Y and Al atoms occupy the Wyckoff positions (1/2,1/2,1/2) and (3/4,3/4,3/4), respectively. Table 1 lists the calculated lattice constant, unit cell volume and bulk modulus of Cr_2MnAl and Cr_2CoAl at external pressures from 0 to 30 GPa at an interval of 5 GPa along with previously available experimental and computational data for comparison. For Cr_2CoAl, the deviations of calculated lattice constant at 0 GPa from the experimental data are 0.98% [14] and 0.38% [15], unfortunately there is no available lattice constant data for Cr_2MnAl to compare.

Other parameters presented in Table 1 show good agreement with the previous reports. Hence these first principles calculations are considered to be reliable. It is evident from Table 1 that the pressure dependent values of lattice constants and unit cell volumes of Cr_2YAl (Y=Mn, Co) decrease gradually with hydrostatic pressure. This implies the structural stability of both the compounds over the studied pressure range (0–30 GPa). Moreover, the phonon dispersion curve helps to examine the dynamical stability of compounds. Figure 2(a)-(h) displays the calculated phonon dispersion curves of Cr_2MnAl and Cr_2CoAl along the high symmetry directions *W-L-Γ-X-W-K* in the Brillouin zone at external pressures from 0 to 30 GPa at an interval of 10 GPa. The absence of any imaginary phonon frequency in the phonon dispersion curves of Cr_2MnAl and Cr_2CoAl at different external pressures indicates their dynamical stability over the studied pressure range.

3.2. Elastic properties

The crystal structure of a material has great influence on the elastic properties which give a relation between its mechanical and dynamical behaviour. DFT calculations are done to study the elastic properties of the Heusler compounds Cr_2YAl (Y=Mn, Co). The calculations are done within Generalized Gradient Approximation. The finite strain theory is applied to calculate the elastic constants of Cr_2YAl (Y=Mn, Co) [31, 32].

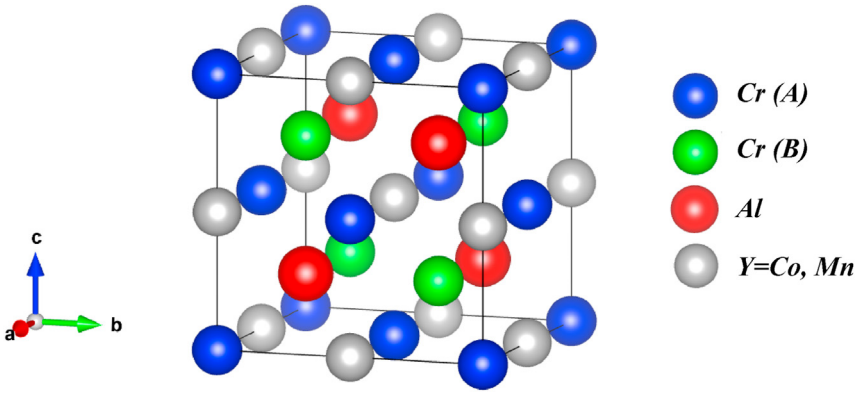

Figure 1. Crystal structure of Cr_2YAl (Y=Mn, Co).

Table 1. Calculated lattice parameters a (Å), unit cell volume V (Å^3) and bulk modulus B (GPa) for Cr_2CoAl and Cr_2MnAl up to pressure (P) 30 GPa.

Compound	P (GPa)	a(Å)	V(Å^3)	B(GPa)	Deviation of lattice constant (%)	Method	Reference
Cr_2CoAl	0	5.794			0.98		Expt. [14]
	0	5.760			0.38		Expt. [15]
	0	5.770			0.55	GGA	[20]
	0	5.738	188.958	228.21		GGA	This work
	5	5.69	184.220	230.18			
	10	5.66	181.321	257.97			
	15	5.62	177.504	290.71			
	20	5.59	174.677	307.98			
	25	5.56	171.880	313.73			
	30	5.53	169.112	331.98			
Cr_2MnAl	0	5.831			0.99	GGA	[5]
	0	5.850			0.67	GGA	[17]
	0	5.866		141.83	0.39	GGA	[22]
	0	5.889	204.23	125.29		GGA	This work
	5	5.82	197.137	159.67			
	10	5.77	192.100	186.68			
	15	5.72	187.149	214.44			
	20	5.68	183.250	236.23			
	25	5.64	179.406	258.07			
	30	5.60	175.616	274.55			

Due to symmetry of cubic structure, the number of independent single crystal elastic constants reduces to three from twenty-one. As both Cr_2MnAl and Cr_2CoAl possess cubic structure, they have three independent elastic constants: C_{11}, C_{12} and C_{44}. Table 2 shows the calculated values of elastic constants C_{11}, C_{12}, C_{44}, Cauchy pressure (C'') and Kleinman parameter (ζ) of Cr_2YAl (Y=Mn, Co) at external pressures from 0 to 30 GPa at an interval of 5 GPa. There is a good agreement between these data with available theoretical studies at 0 GPa C'' and ζ are calculated from the formulas mentioned below:

$$C'' = C_{12} - C_{44} \tag{1}$$

$$\zeta = \frac{C_{11} + 8C_{12}}{7C_{11} + 2C_{12}} \tag{2}$$

In order to be regarded as mechanically stable compound, Cr_2MnAl and Cr_2CoAl have to satisfy the stability criteria for cubic crystal [33]:

$$C_{11} + 2C_{12} > 0,$$

$$C_{44} > 0,$$

$$C_{11} - C_{12} > 0$$

Mechanical stability of the compounds Cr_2YAl (Y=Mn, Co) is confirmed from the calculated values of elastic constants C_{11}, C_{12}, C_{44}. At pressure P, the cubic structure has to satisfy the following the mechanical stability criteria [34]:

$$(C_{11} + 2C_{12})/3 + P/3 > 0,$$

$$C_{44} - P > 0,$$

$$(C_{11} - C_{12})/2 - P > 0$$

Hence the mechanical stability of both Cr_2MnAl and Cr_2CoAl is not interrupted in the studied pressure range (0–30 GPa) which is confirmed from the calculated values of single crystal elastic constants. The elastic constant C_{11} signifies the unidirectional compression along the crystallographic direction while C_{44} measures the response to the shear deformation. It is observed from Table 2 that $C_{11} > C_{44}$ in the whole pressure range which indicates the difficulty in unidirectional deformation compared to the shear deformation. The unidirectional compression along the crystallographic direction increases with hydrostatic pressure over the studied pressure range. For both Cr_2CoAl and Cr_2MnAl, the value of C_{44} also increases with pressure up to 30 GPa which indicates the increasing response of the compounds to shear deformation.

The variations of single crystal elastic constants (C_{11}, C_{12}, C_{44}) with pressure are presented by bar graphs in Figure 3(a)-(c) at external pressures from 0 to 30 GPa at an interval of 5 GPa.

Calculated values of bulk modulus B, shear modulus G, Young's modulus Y, Pugh's ratio k, Poisson's ratio υ, machinability μ, Vickers hardness H_V at external pressures from 0 to 30 GPa at an interval of 5 GPa are listed in Table 3. These parameters are calculated by using the following formula [32, 35]:

$$B = \frac{B_V + B_R}{2} \tag{3}$$

B, B_V and B_R represents bulk moduli according to Hill-Voigt-Reuss.

$$G = \frac{G_V + G_R}{2} \tag{4}$$

G, G_V and G_R represents shear moduli according to Hill-Voigt-Reuss.

$$Y = \frac{9BG}{3B + G} \tag{5}$$

$$\upsilon = \frac{3B - 2G}{6B + 2G} \tag{6}$$

$$H_V = \frac{(1 - 2\upsilon)Y}{6(1 + \upsilon)} \tag{7}$$

$$k = \frac{G}{B} \tag{8}$$

$$\mu = \frac{B}{C_{44}} \tag{9}$$

The elastic modulus suggested by Hill is the average of the moduli suggested by Voigt and Reuss [35]. Strain distribution is assumed to be

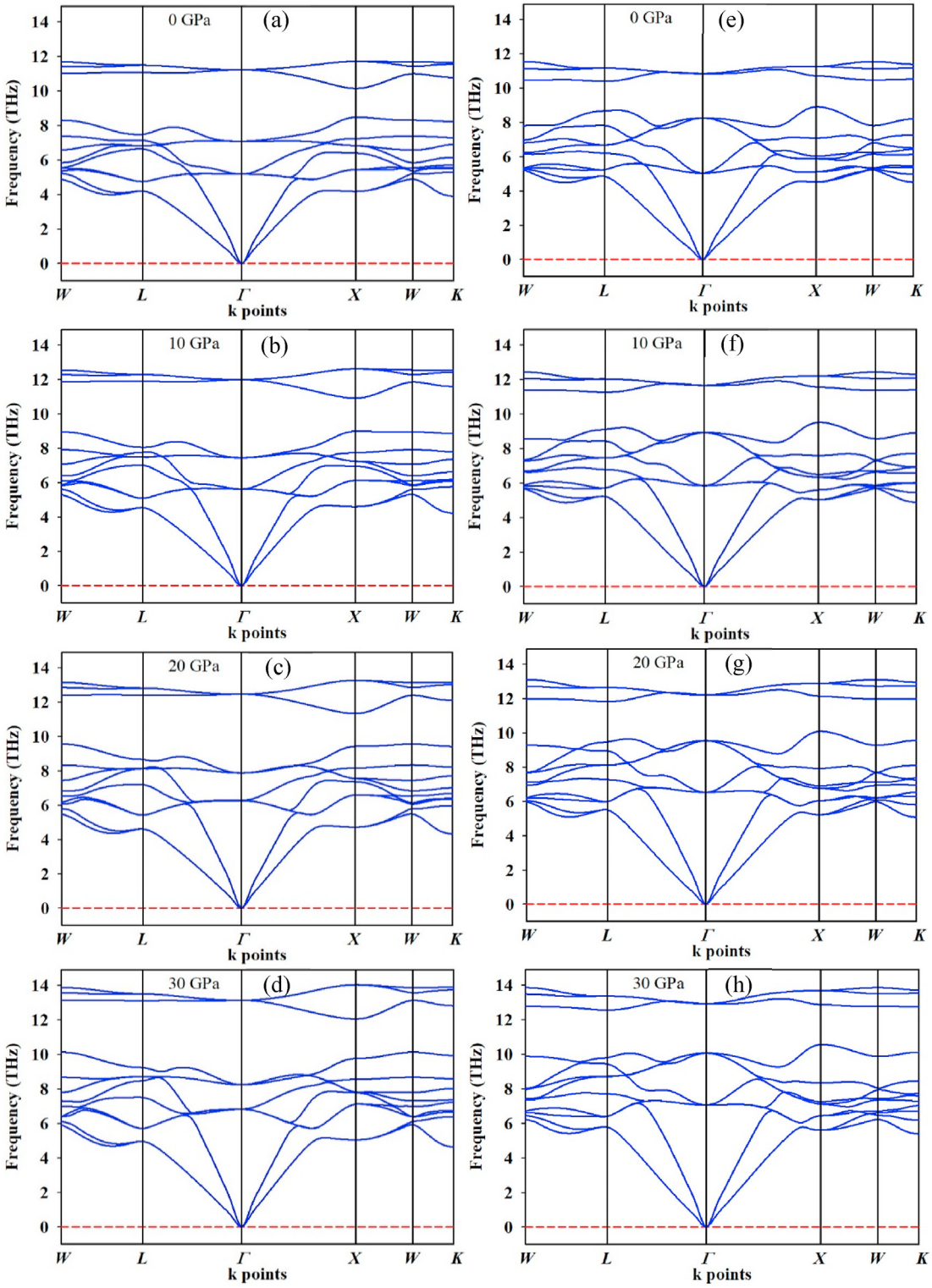

Figure 2. Phonon dispersion curves of the considered compounds along the high symmetry directions W-L-Γ-X-W-K. Calculated phonon dispersion of Cr_2MnAl at pressures (a) 0 GPa, (b) 10 GPa, (c) 20 GPa and (d) 30 GPa. Calculated phonon dispersion of Cr_2CoAl at (e) 0 GPa, (f) 10 GPa, (g) 20 GPa and (h) 30 GPa.

continuous in Voigt approximation, while Reuss assumes discontinuity in strain distribution [36]. On the other hand, stress distribution is approximated to be discontinuous in Voigt approximation and continuous in Reuss approximation. For both the compounds Cr_2MnAl and Cr_2CoAl, the lower value of G (87.62 and 96.25 GPa for Cr_2MnAl and Cr_2CoAl, respectively) as compared to that of B (125.29 and 228.21 GPa for Cr_2MnAl and Cr_2CoAl, respectively) indicates the dominance to the failure of the materials through shear deformation. Young's modulus measures the stiffness against longitudinal deformation [37, 38]. It is also a significant parameter to measure thermal shock resistance of a

Table 2. Calculated elastic constants C_{ij} (GPa), Cauchy pressure C'' (GPa) and Kleinman parameter ζ of Cr_2YAl (Y=Mn, Co) up to pressure (P) 30 GPa.

Compound	P	C_{11}	C_{12}	C_{44}	C''	ζ	Reference
Cr_2CoAl	0	345.29	169.68	103.58	66.110	0.618	This work
	5	355.37	167.59	104.92	62.670	0.601	
	10	390.95	191.47	112.83	78.640	0.616	
	15	431.33	220.39	120.55	99.840	0.634	
	20	455.86	234.05	127.91	106.140	0.636	
	25	468.69	236.25	134.66	101.590	0.628	
	30	493.73	251.11	141.27	109.840	0.632	
Cr_2MnAl	0	246	89.70	104.60			[22]
	0	218.39	78.74	101.99	-23.250	0.503	This work
	5	263.85	107.58	117.30	-9.720	0.545	
	10	299.69	130.17	129.51	0.660	0.569	
	15	336.12	153.60	140.01	13.590	0.588	
	20	365.19	171.74	149.11	22.630	0.600	
	25	393.28	190.46	157.25	33.210	0.612	
	30	415.6	204.04	164.34	39.700	0.617	

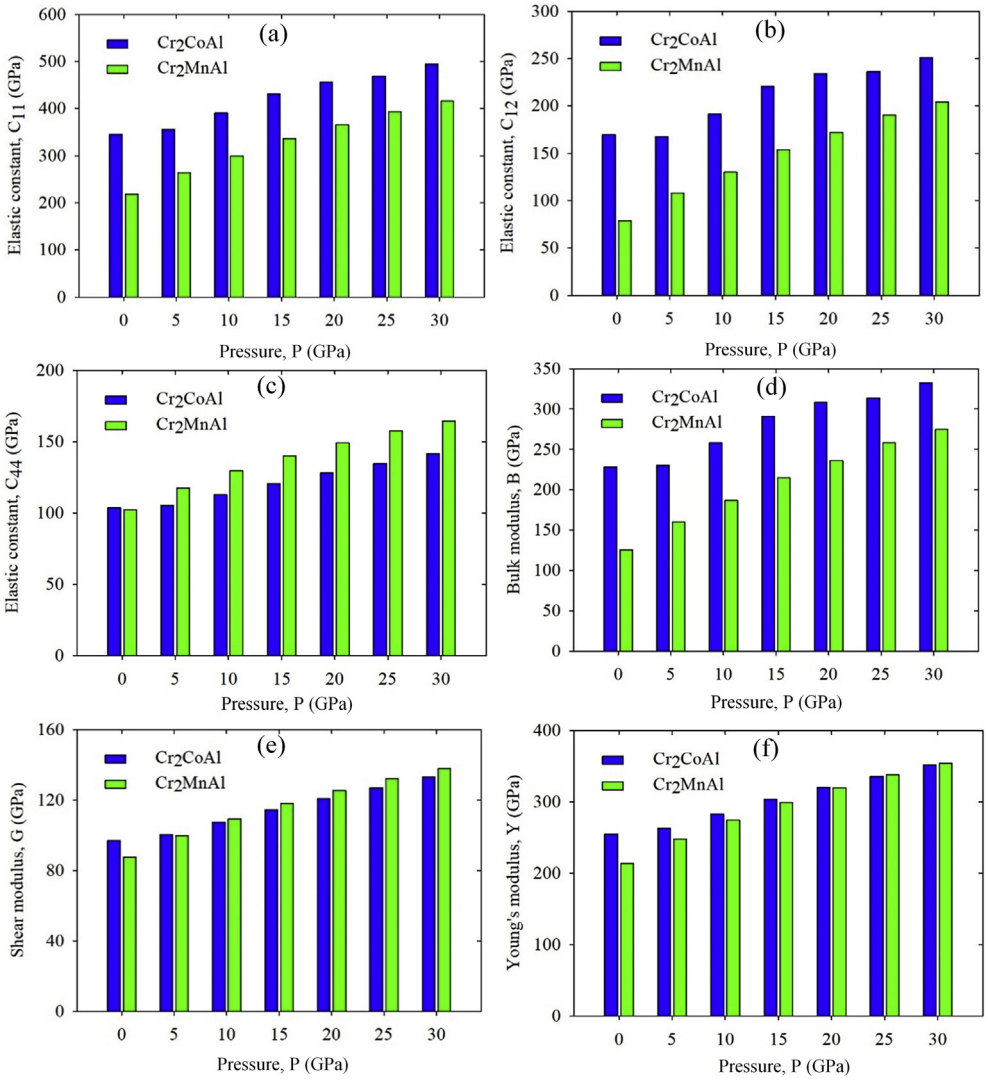

Figure 3. Pressure dependence of elastic constants (a) C_{11}, (b) C_{12}, (c) C_{44}, (d) B, (e) G, (f) Y of Cr_2YAl (Y=Mn, Co) from 0 to 30 GPa at an interval of 5 GPa.

material. The larger the value of Young's modulus, the smaller the thermal shock resistance. Thermal shock resistance of Cr_2MnAl is larger than that of Cr_2CoAl.

The variations of B, G and Y with pressure are also presented by bar graphs in Figure 3(d)–(f) at external pressures from 0 to 30 GPa at an interval of 5 GPa. It is evident from Table 2, Table 3 and Figure 3(a)–(f)

Table 3. Calculated bulk modulus B (GPa), shear modulus G (GPa), Young's modulus Y (GPa), Pugh's ratio k or G/B, and Poisson's ratio υ, machinability μ and Vickers hardness H_v of Cr_2YAl (Y=Mn, Co) up to pressure (P) 30 GPa.

Compound	P	B	G	Y	G/B	υ	μ	H_v	Reference
Cr_2CoAl	0	228.21	96.95	254.77	0.425	0.314	2.203	12.026	This work
	5	230.18	100.36	262.87	0.436	0.310	2.194	12.735	
	10	257.97	107.40	282.94	0.416	0.317	2.286	13.088	
	15	290.71	114.27	303.10	0.393	0.326	2.412	13.238	
	20	307.98	120.82	320.54	0.392	0.327	2.408	13.972	
	25	313.73	126.96	335.61	0.405	0.322	2.330	15.090	
	30	331.98	132.91	351.78	0.400	0.323	2.350	15.649	
Cr_2MnAl	0	142	93	229	0.66				[22]
	0	125.29	87.62	213.17	0.699	0.216	1.228	16.564	This work
	5	159.67	99.67	247.51	0.624	0.242	1.361	17.167	
	10	186.68	109.27	274.29	0.585	0.255	1.441	17.839	
	15	214.44	117.93	298.98	0.550	0.268	1.532	18.269	
	20	236.23	125.35	319.53	0.531	0.275	1.584	18.839	
	25	258.07	131.89	338.08	0.511	0.282	1.641	19.198	
	30	274.55	137.7	353.93	0.502	0.285	1.671	19.724	

that C_{11}, C_{12}, C_{44} and B, G, Y increase gradually with pressure for both Cr_2MnAl and Cr_2CoAl suggesting that these compounds are mechanically stable over the studied pressure range.

Ductility and brittleness of a compound is determined by various parameters such as Pugh's ratio [39], Poisson's ratio [40] and Cauchy pressure [41]. The ductility and brittleness limits are as follows: 0.5 is the limit for Pugh's ratio (G/B), 0.31 is the limit for Poisson's ratio and positive value of Cauchy pressure is the indicator of ductility. A compound having Pugh's ratio less than 0.5 is regarded as a ductile one. Hence Cr_2CoAl is ductile but Cr_2MnAl is brittle in nature which is evident from the values of Pugh's ratio shown in Table 3. The value of Poisson's ratio υ has to be larger than 0.31 for a ductile material. So that Cr_2MnAl is brittle while Cr_2CoAl is ductile according to this criterion. The value of Cauchy pressure is positive for the compound Cr_2CoAl which indicates the ductile nature of this compound. On the other hand, negative value of Cauchy pressure points out the brittleness of Cr_2MnAl.

The value of Poisson's ratio υ also indicates the type of bonding in a compound. The values of υ are 0.10, 0.25 and 0.33 which correspond to the dominance of covalent, ionic and metallic bonding, respectively. The value of υ is 0.314 for Cr_2CoAl which indicates the dominant metallic nature. On the other hand, $\upsilon = 0.216$ corresponds to the mixture of covalent and ionic bonding in Cr_2MnAl having slight dominance of ionic contribution. The covalent nature of Cr_2MnAl vanishes with increasing pressure while metallic contribution is evident for Cr_2CoAl over the entire pressure range.

Kleinman parameter ζ [42] indicates the type of bonding in a compound. The contribution of bond bending or bond stretching to withstand the external pressure is determined by the value of ζ. The value $\zeta = 0$ corresponds to the dominance of bond stretching while $\zeta = 1$ corresponds to the dominance of bond bending. Strength of Cr_2CoAl is dominated by bond bending which is evident from the value of ζ [cf. Table 2]. On the other hand, almost equal contribution of bond bending and bond stretching to the strength of Cr_2MnAl is expected from the value of ζ. ζ is pressure dependent. A gradual increase of this parameter with hydrostatic pressure is observed for Cr_2MnAl while anomalous behaviour is observed for Cr_2CoAl [cf. Table 2]. This implies that bond bending contribution to the strength of Cr_2MnAl increases progressively with pressure.

Machinability index μ is used to judge the industrial applicability of a compound. A material is regarded as good in cutting if its machinability index is large. The values of μ for Cr_2MnAl and Cr_2CoAl are 1.228 and 2.203, respectively. This indicates that Cr_2CoAl is more machinable than Cr_2MnAl. A smooth increase in machinability with pressure is observed for Cr_2MnAl while the behaviour of Cr_2CoAl in terms of machinability is abrupt over the studied pressure range.

Vickers Hardness of the compounds Cr_2MnAl and Cr_2CoAl [43, 44] is calculated by using formula (7). The hardness values presented in Table 3 indicates that Cr_2MnAl is harder than Cr_2CoAl. This implies that Cr_2MnAl resists more plastic deformation as compared to Cr_2CoAl. It is also observed that both the compounds become harder with increasing pressure over the studied range.

3.3. Debye temperature and ultrasonic properties

Table 4 presents the calculated values of density ρ, Debye temperature θ_D, longitudinal sound velocity v_l, shear sound velocity v_t and average sound velocity v_m for the Heusler alloys Cr_2MnAl and Cr_2CoAl.

Debye temperature is a very important parameter which is used to interpret various properties such as thermal conductivity, melting temperature etc. Average sound velocity v_m, which is required to determine Debye temperature can be calculated from the values of elastic constants. The formulas which are used to calculate Debye temperature θ_D, longitudinal sound velocity v_l, shear sound velocity v_t and average sound velocity v_m are as follows [45]:

$$\theta_D = \frac{h}{k_B}\left[\frac{3n}{4\pi}\left(\frac{\rho N_A}{M}\right)\right]^{\frac{1}{3}} v_m \tag{10}$$

$$v_m = \left[\frac{1}{3}\left(\frac{2}{v_t^3} + \frac{1}{v_l^3}\right)\right]^{-\frac{1}{3}} \tag{11}$$

$$v_l = \sqrt{\frac{3B + 4G}{3\rho}} \tag{12}$$

$$v_t = \sqrt{\frac{G}{\rho}} \tag{13}$$

where h is Planck's constant is, k_B Boltzmann's constant, n is the number of atoms in the molecule, ρ is the density, N_A is the Avogadro number and M is the molecular weight.

Hardness of a compound is related to the Debye temperature. The higher the Debye temperature, the harder the compound. The values of Debye temperature are 848.2 K and 901.29 K for Cr_2MnAl and Cr_2CoAl,

Table 4. Calculated ρ (gm/cm^3), isotropic acoustic velocities (v_l, v_t, v_m in kms^{-1}), Debye temperature (θ_D in K) of Cr_2YAl (Y=Mn, Co) up to pressure (P) 30 GPa.

Compound	P	ρ	v_l	v_t	v_m	θ_D	Reference
Cr_2CoAl	0	6.671	26.5330	3.8120	4.3610	901.29	This work
	5	6.845	26.6475	3.8290	4.3810	920.95	
	10	6.955	28.1869	3.9298	4.4965	955.26	
	15	7.104	29.8928	4.0106	4.5892	988.89	
	20	7.219	30.7613	4.0910	4.6812	1019.57	
	25	7.337	31.0526	4.1599	4.7600	1047.97	
	30	7.457	31.9328	4.2219	4.8310	1075.16	
Cr_2MnAl	0	6.042	19.8798	3.8083	4.3543	848.20	This work
	5	6.262	22.3659	3.9895	4.5625	910.23	
	10	6.426	24.1394	4.1235	4.7163	957.33	
	15	6.596	25.8294	4.2282	4.8366	998.98	
	20	6.737	27.0832	4.3136	4.9345	1033.61	
	25	6.881	28.2801	4.3780	5.0085	1064.04	
	30	7.030	29.1508	4.4259	5.0634	1091.14	

respectively [cf. Table 4]. Hence large value of Debye temperature corresponds to high degree of hardness of the Heusler alloys Cr_2MnAl and Cr_2CoAl. The increase of the Debye temperature with increase of hydrostatic pressure indicates the crystal stiffening of both the compounds.

3.4. Electronic properties

Band structure, total and partial density of state calculations is important to study electronic properties of the compounds Cr_2MnAl and Cr_2CoAl. Optical properties of a compound are directly related to the band structure of the compound. Electronic band structure is calculated at zero pressure along the high symmetry directions *W-L-Γ-X-W-K* in the first Brillouin zone. Figure 4(a)-(d) and 4(e)-(h) show the band structures of Cr_2CoAl at external pressures from 0 to 30 GPa at an interval of 10 GPa for spin-up and spin-down channels, respectively. The Fermi level (E_F) is represented by the horizontal dashed line. The calculated band structures of Cr_2CoAl for spin-up and spin-down channels are consistent with the previous computational study [21]. It is evident from the band diagram, Figure 4(a) that there is a band gap near E_F, suggesting the non-metallic nature of Cr_2CoAl for spin-up channel.

On the other hand, the band structure with no band gap as shown in Figure 4(e) indicates the metallic nature of Cr_2CoAl for spin-down channel. This happens because of the crossing of bands at E_F. Hence band structure of the Heusler compound Cr_2CoAl confirms the near half metallicity of this compound. It is relevant to mention that a compound is regarded as near half-metal if a band gap is observed outside the Fermi level in the band structure for one of the spin channels or the DOS at E_F is very small [5]. The band gap of Cr_2CoAl for up spin channel is found 0.13 eV at 0 GPa and increases with the increase of pressure up to 20 GPa Figure 4(a)–(d). Above 20 GPa the band gap reduces to zero. On the other hand, the metallic nature of Cr_2CoAl for down spin channel retain up to pressure 30 GPa [Figure 4(e)–(h)]. So the near half-metallic character of Cr_2CoAl seems to be suppressed by external pressure at around 30 GPa and therefore the compound becomes metallic.

In order to interpret the contributions of individual atoms to the total density of states (TDOS), the partial density of states (PDOS) for the atoms constituting the structure are calculated. Figure 5(a) represents the TDOS and PDOS of the compound Cr_2CoAl for both up and down-spin channels. The Fermi level is represented by the vertical dotted line (red colour) at 0 eV. PDOS of Cr, Co, Al are calculated to describe the contribution of these atoms to the TDOS of Cr_2CoAl. Firstly, TDOS and PDOS of Cr_2CoAl for the up spin are described in which positive value of DOS is for spin-up electrons. At the E_F, value of TDOS is negligible, which indicates non-metallic behaviour of the compound Cr_2CoAl for up-spin channel. It is noticeable that there is no contribution from the orbitals of Al to the TDOS. Here, contribution of Co 3*d* state to the TDOS below the E_F is significant along with the contribution from Cr 3*d* state. Another remarkable feature of the TDOS curve is the presence of a peak above the E_F at 2 eV which arises mainly due to Cr 3*d* orbital.

On the other hand, negative value of DOS is for spin-down electrons in the TDOS and PDOS curves. At E_F, high value of TDOS is evident which confirms the metallic nature of Cr_2CoAl for spin down channel. The contributions to the TDOS at E_F originate from Cr 3*d* and Co 3*d* states. It is noticeable that there is no contribution from the orbital of Al atom to the TDOS at E_F. There is a pseudogap at the left of E_F which indicates the stability of the structure [46]. The valence band just below E_F extends from -5.4 to -1 eV. Here TDOS has significant contributions from Cr 3*d* and Co 3*d* states. In this band, little contribution comes from the Al atom. Here, strong hybridization of Co 3*d* and Cr 3*d* states to the TDOS below E_F is observed. There is a peak above E_F at an energy of 1.9 eV. This peak is due to sole contribution from Cr 3*d* orbital. The near half metallicity of Cr_2CoAl is evident from the band structure and DOS curves. The pressure dependent TDOS curve of Cr_2CoAl [Figure 5(c)] shows that the near half metallicity disappears at ~30 GPa because TDOS at E_F is non-zero at this pressure for both up and down spin channels.

Electronic band structure of Cr_2MnAl is calculated at pressures up to 30 GPa at an interval of 10 GPa along the high symmetry directions *W-L-Γ-X-W-K* in the first Brillouin zone. Figure 6 (a-d) and (e-h) represent the band structures of Cr_2MnAl for up and down spin, respectively. There is a band gap in the band structure for up spin channel. This implies that Cr_2MnAl is semiconducting in nature for one type of spin, namely, up spin. On the other hand, overlapping of the valence band and conduction band is observed from Figure 6(e) at E_F in the band structure for other type of spin, namely, down spin. This indicates the metallic nature of Cr_2MnAl for down spin channel. Hence half metallicity of Cr_2MnAl is revealed from the band structures for up and down spin channels. This result is consistent with the available computational investigation [22]. The value of band gap of Cr_2MnAl at 0 GPa is 0.38 eV for up spin channel. The band gap decreases with increasing external pressure and become *zero* at pressure around 30 GPa. On the other hand, for down spin channel the metallic character of Cr_2MnAl is preserved up to 30 GPa. It seems that the half-metallicity of Cr_2MnAl disappears at around 30 GPa.

Figure 5(b) shows the TDOS and PDOS of Cr_2MnAl for up and down spin channels at zero pressure. The Fermi level is indicated by vertical broken line marked as red. The value of TDOS is zero for up spin which is evident from Figure 5(b). This implies that Cr_2MnAl is semiconducting in

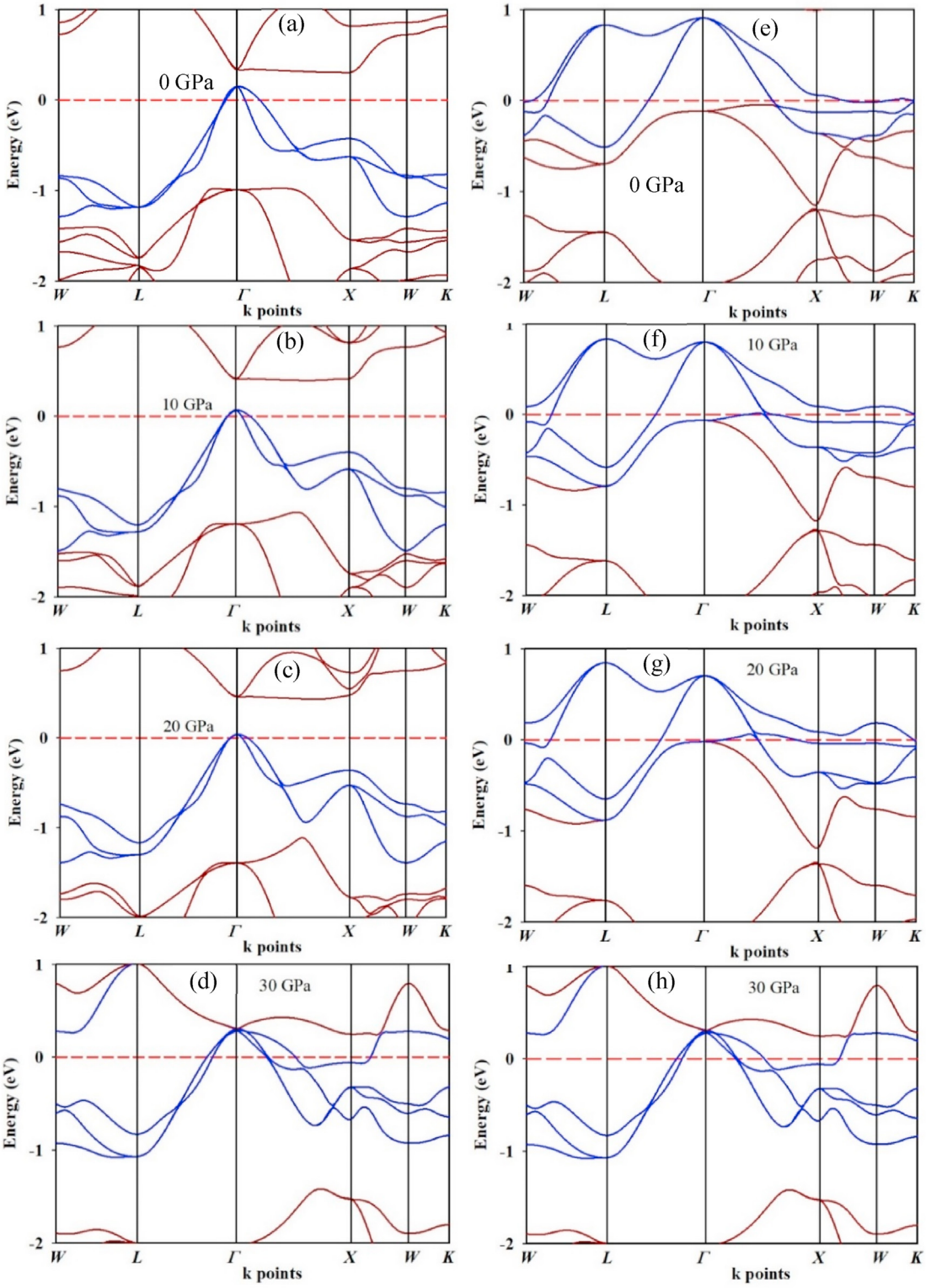

Figure 4. Band structure of Cr_2CoAl along the high symmetry directions W-L-Γ-X-W-K. Horizontal broken line (red colour) indicates the Fermi level. Calculated band structure for spin-up channel at pressures (a) 0 GPa, (b) 10 GPa, (c) 20 GPa and (d) 30 GPa. Band structure for spin-down channel at (e) 0 GPa, (f) 10 GPa, (g) 20 GPa and (h) 30 GPa.

nature for up spin. Above E_F, a peak is observed at 1.4 eV in which Cr 3*d* state contributes more than other states of Mn and Al atoms.

But the finite value of TDOS points out the metallic nature of Cr_2MnAl for other type of spin, namely, down spin. Hence the TDOS curve also confirms the half metallic behaviour of the compound Cr_2MnAl. For the down spin channel, the dominant contribution to the TDOS at E_F comes from Cr 3*d* and Mn 3*d* states. The Al 3*p* state has almost no contribution to the TDOS at E_F. There is deep valley at the left of E_F known as pseudogap indicates the structural stability of the structure [46]. There is a peak in the TDOS curve at about -2.2 eV which is originated from the

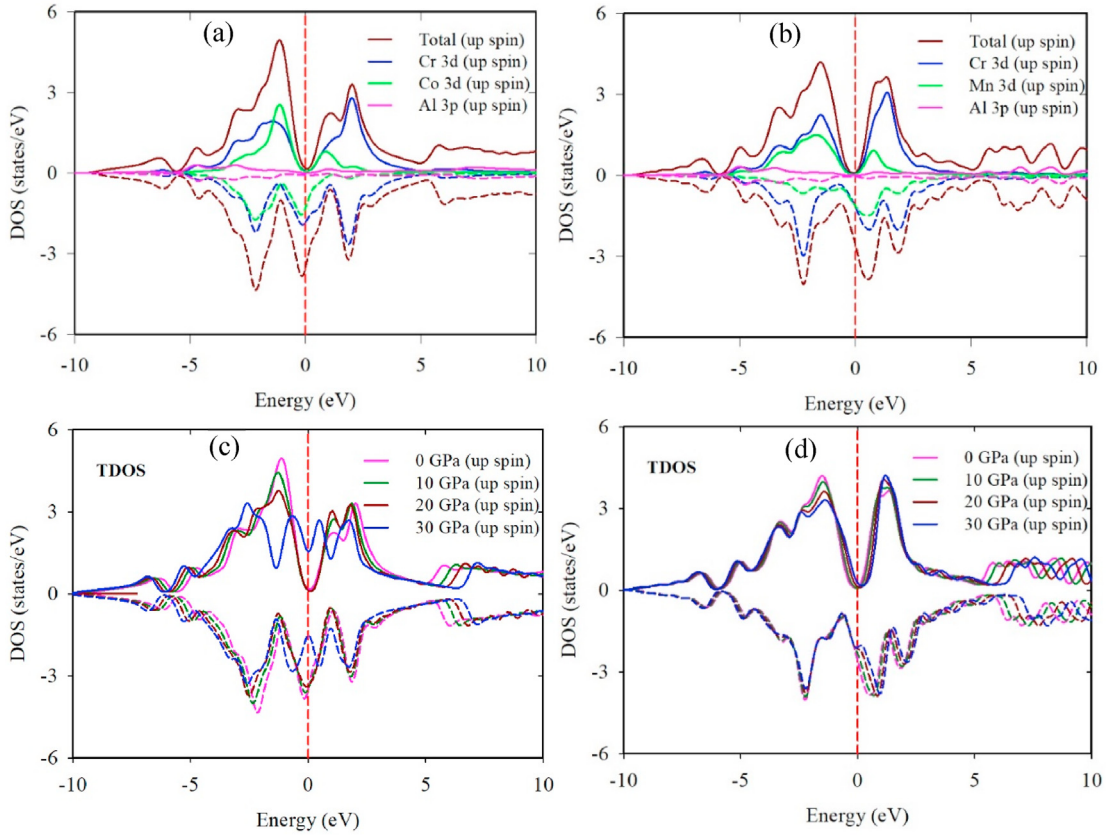

Figure 5. TDOS and PDOS of the compounds (a) Cr_2CoAl and (b) Cr_2MnAl at 0 GPa, and TDOS of (c) Cr_2CoAl and (d) Cr_2MnAl at pressures from 0 to 30 GPa at an interval of 10 GPa. The vertical broken line (red colour) indicates the Fermi level. Solid and dashed lines indicate DOS for spin up and down channels, respectively.

hybridization of Cr 3*d* and Mn 3*d* states with the dominance of Cr 3*d* state. Two more peaks above E_F are seen at about 0.5 eV and 1.8 eV which are Cr 3*d* dominated. Moreover, the half metallicity of Cr_2MnAl is confirmed from both the band structure and TDOS curves. It is noteworthy that these interpretations of the band structure and TDOS curves are also helpful to explain the optical properties of Cr_2MnAl which will be discussed in Section 3.5.

In addition, the pressure dependence of TDOS of Cr_2MnAl [Figure 5(d)] shows that the TDOS at E_F for up spin channel changes from zero to finite value at around 30 GPa whereas TDOS at E_F for down spin channel is non-zero at pressures up to 30 GPa. Hence half metallicity of Cr_2MnAl is lost at ~30 GPa.

In order to observe the effect of Hubbard parameter (U), the band structure of Cr_2MnAl and Cr_2CoAl are also calculated by using GGA + U approximations as shown in Figures 7 and 8, respectively. The same value of U (0.5 eV–6.0 eV at an interval of 0.5 eV) is considered for Cr and Mn (Co) atoms respectively for Cr_2MnAl (Cr_2CoAl) for a particular calculation. Here the band structures are shown only for U = 0.5 eV and 1.0 eV (Figures 7 and 8). Our calculation suggests that the half-metallicity of Cr_2MnAl starts to diminish at U~0.5 eV [Figure 7]. On the other hand, the near half-metallicity of Cr_2CoAl is retained for U ~ 0.5 eV and it is disappeared at the value of U ~ 1.0 eV as shown in Figure 8. The band structure for higher U (>1.0 eV) is not presented here, since the band structure characteristics shown by both the compounds for U~1.0 eV remain same up to the maximum considered U value of 6.0 eV.

The magnetic moments of Cr_2YAl (Mn, Co) are calculated from the spin projected integrated DOS [47]. The calculated total magnetic moments are 0.18 μ_B and 1.86 μ_B per formula unit for Cr_2CoAl and Cr_2MnAl respectively.

3.5. Optical properties

Various energy dependent optical parameters such as the real and imaginary parts of dielectric constant, $\varepsilon_1(\omega)$ and $\varepsilon_2(\omega)$, respectively, static refractive index *n*, extinction coefficient *k*, loss function *L*, real part of the optical conductivity σ, reflectivity *R* and the absorption coefficient α , are calculated at pressures up to 30 GPa at an interval of 10 GPa to study the response of a material to incident electromagnetic waves, namely, infrared, visible and ultraviolet radiations. These studies are helpful to judge the potential optoelectronic device applications. The calculated optical parameters for Cr_2MnAl and Cr_2CoAl at external pressures up to 30 GPa are presented in Figures 9, 10, 11, 12, 13, and 14. The local field effect is not included in this calculation. A plasma frequency of 3 eV, damping of 0.05 eV is used for the dielectric constant calculation [48]. The $\varepsilon_1(\omega)$ and $\varepsilon_2(\omega)$ are connected with each other through Kramers Kronig relation.

The $\varepsilon_2(\omega)$ is given by the equation [49]:

$$\varepsilon_2(\omega) = \frac{2e^2\pi}{\Omega\varepsilon_0}\sum_{k,v,c}\left|\langle\psi_k^c|u\cdot r|\psi_k^v\rangle\right|^2\delta\left(E_k^c - E_k^v - E\right) \tag{14}$$

where *e* is the electronic charge, Ω is the volume of the unit cell, *u* is the unit vector along the polarization of the incident electric field, ω is the frequency of the photon, ψ_k^c and ψ_k^v are the wave functions for conduction and valence band electrons. The other optical constants are directly related to $\varepsilon_2(\omega)$.

The static refractive index $n(\omega)$, extinction coefficient $k(\omega)$, absorption coefficient $\alpha(\omega)$, loss function $L(\omega)$, reflectivity $R(\omega)$, and photoconductivity $\sigma(\omega)$ can be calculated by using the equations [49, 50]:

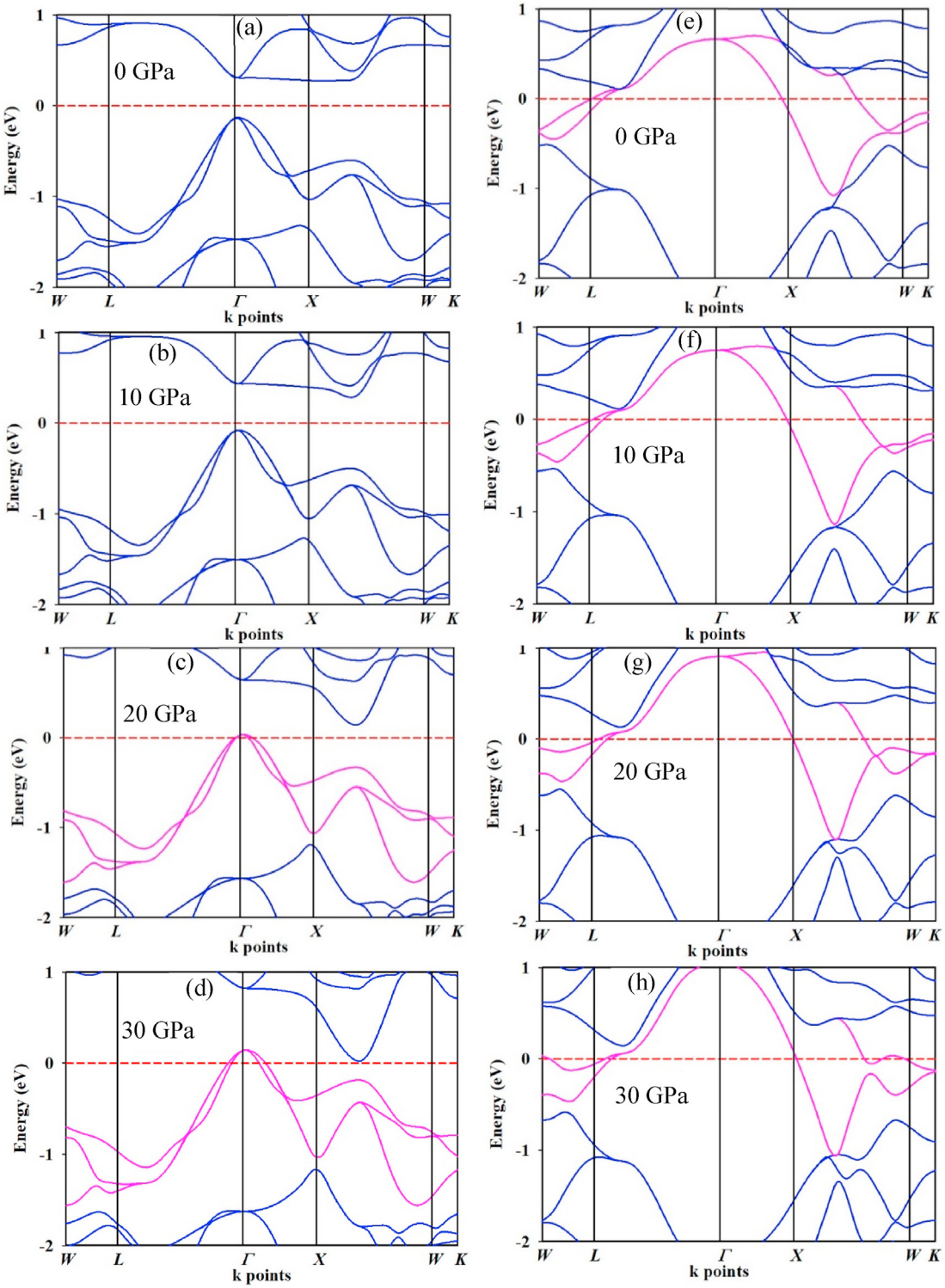

Figure 6. Band structure of Cr_2MnAl along the high symmetry directions W-L-Γ-X-W-K. Horizontal broken line (red colour) indicates the Fermi level. Calculated band structure for spin-up channel at pressures (a) 0 GPa, (b) 10 GPa, (c) 20 GPa and (d) 30 GPa. Band structure for spin-down channel at pressures (e) 0 GPa, (f) 10 GPa, (g) 20 GPa and (h) 30 GPa.

$$n(\omega)=\frac{1}{\sqrt{2}}\left[\sqrt{\{\varepsilon_1(\omega)\}^2+\{\varepsilon_2(\omega)\}^2}+\varepsilon_1(\omega)\right]^{\frac{1}{2}} \quad (15)$$

$$k(\omega)=\frac{1}{\sqrt{2}}\left[\sqrt{\{\varepsilon_1(\omega)\}^2+\{\varepsilon_2(\omega)\}^2}-\varepsilon_1(\omega)\right]^{\frac{1}{2}} \quad (16)$$

$$\alpha(\omega)=\sqrt{2}\omega\left[\sqrt{\{\varepsilon_1(\omega)\}^2+\{\varepsilon_2(\omega)\}^2}-\varepsilon_1(\omega)\right]^{\frac{1}{2}} \quad (17)$$

$$L(\omega)=\frac{\varepsilon_2(\omega)}{\left[\{\varepsilon_1(\omega)\}^2+\{\varepsilon_2(\omega)\}^2\right]} \quad (18)$$

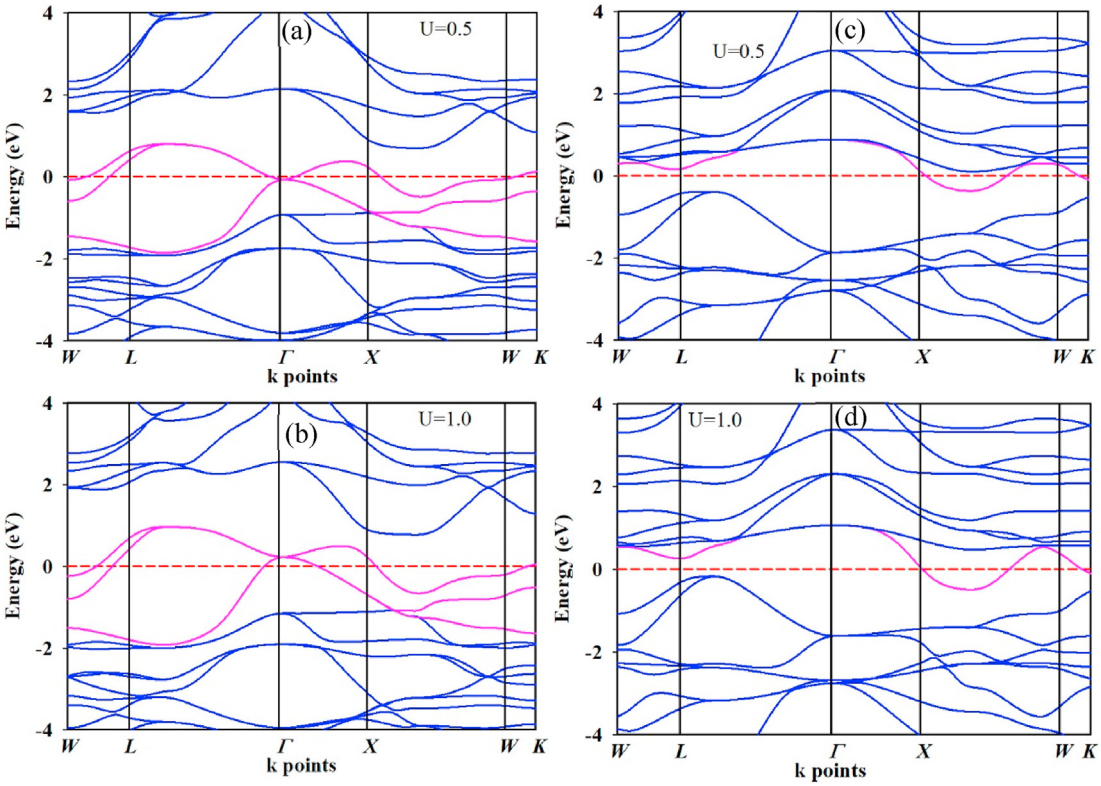

Figure 7. Band structure of Cr_2MnAl with DFT + U approximation along the high symmetry directions W-L-Γ-X-W-K. Horizontal broken line (red colour) indicates the Fermi level. Calculated band structure for spin-up channel considering (a) U = 0.5 eV, (b) U = 1.0 eV and for spin-down channel considering (c) U = 0.5 eV, (d) U = 1.0 eV for both Cr and Mn atoms.

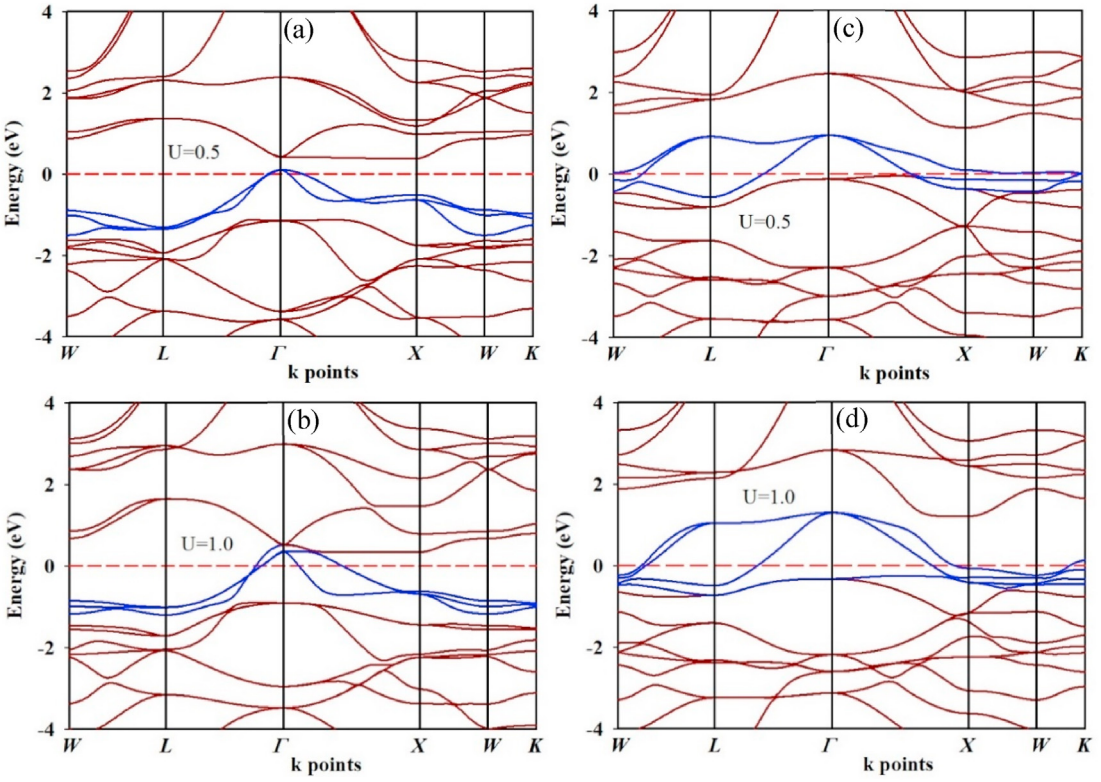

Figure 8. Band structure of Cr_2CoAl with DFT + U approximation along the high symmetry directions W-L-Γ-X-W-K. Horizontal broken line (red colour) indicates the Fermi level. Calculated band structure for spin-up channel considering (a) U = 0.5 eV, (b) U = 1.0 eV and for spin-down channel considering (c) U = 0.5 eV, (d) U = 1.0 eV for both Cr and Co atoms.

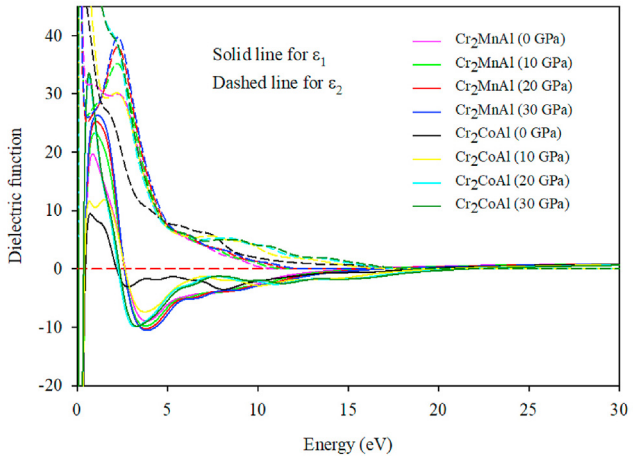

Figure 9. Real (ε_1) and imaginary part (ε_2) of dielectric function of Cr_2MnAl and Cr_2CoAl at pressures from 0 to 30 GPa at an interval of 10 GPa.

$$R(\omega) = \left| \frac{\sqrt{\varepsilon(\omega)} - 1}{\sqrt{\varepsilon(\omega)} + 1} \right|^2 \tag{19}$$

$$\sigma(\omega) = \frac{\omega \varepsilon_2}{4\pi} \tag{20}$$

Figure 9 represents the variation of $\varepsilon_1(\omega)$ and $\varepsilon_2(\omega)$ with the energy of electromagnetic radiation at pressures from 0 to 30 GPa at an interval of 10 GPa. For metallic compounds, the $\varepsilon_1(\omega)$ should have large negative value. For both Cr_2MnAl and Cr_2CoAl, this behaviour is evident from the patterns shown in Figure 9. It is observed that there is a sharp decrease in ε_1 at about the energy in the range 2–3 eV which is consistent with the DOS curves for Cr_2MnAl and Cr_2CoAl. The relative height of the peaks at around 2 eV at 0 GPa are different for different compounds and the peak heights are seen to increase with pressure up to 30 GPa. The value of ε_2 at 0 GPa approaches zero at about 17 eV and 11 eV for Cr_2CoAl and Cr_2MnAl, respectively, which indicates the sharp decrease in absorption and reflectivity spectra as shown in Figures 11 and 13.

The static refractive index, $n(\omega)$ and extinction coefficient, $k(\omega)$ depend on the wavelength, i.e., energy of the incident radiation. Their dependence on energy of the incident radiation at pressure up to 30 GPa is shown in Figures 10 and 11. The energy dependence of $n(\omega)$ and $k(\omega)$ is very much similar to that of $\varepsilon_2(\omega)$. The static refractive index has the high value of 84.7 and 84.5 at zero photon energy for Cr_2CoAl and Cr_2MnAl,

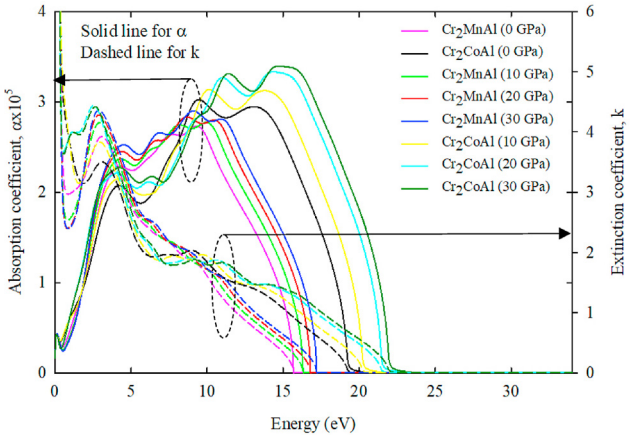

Figure 11. Extinction coefficient (k) and absorption coefficient (α) of Cr_2MnAl and Cr_2CoAl at pressures from 0 to 30 GPa at an interval of 10 GPa.

respectively. Hence these materials are promising candidates for opto-electronic device. The static refractive index for Cr_2CoAl and Cr_2MnAl is roughly unchanged with increasing external pressure. There is a gradual decrease in $n(\omega)$ with the energy and $n(\omega)$ approaches zero at about 17 eV and 11 eV at 0 GPa for Cr_2CoAl and Cr_2MnAl, respectively. This feature is consistent with the dielctric function curves. The static refractive index has the link with the phase velocity of the electromagnetic radiation in the material.

On the other hand, extinction coefficient indicates the attenuation of the electromagnetic radiation in the medium. The extinction coefficient, $k(\omega)$ depends on the wavelength of the incident electromagnetic radiation at different ptressures in the way shown in Figure 11. There is a gradual decrease in $k(\omega)$ with incident energy and finally approaches to zero. There is a peak in the spectrum at 3 eV with different heights for Cr_2MnAl and Cr_2CoAl. The peak heights are seen to increase with increasing external pressure up to 30 GPa for both the compounds.

In the absorption spectrum, Figure 11, a finite value of $\alpha(cm^{-1})$ at zero photon energy indicates the metallic behaviour of the Heusler alloys Cr_2MnAl and Cr_2CoAl. It is also evident from this curve that the absorption decreases sharply to zero at about 19 eV which is expected from the nature of the curve of $\varepsilon_2(\omega)$ for Cr_2CoAl. However, same behaviour is observed for Cr_2MnAl and the value of the absorption coefficient reaches zero at 16 eV. The photon energy at which α approaches zero shifts towards the higher energy with increasing external pressure up to 30 GPa. Overall pressure effect on α looks similar in both compounds.

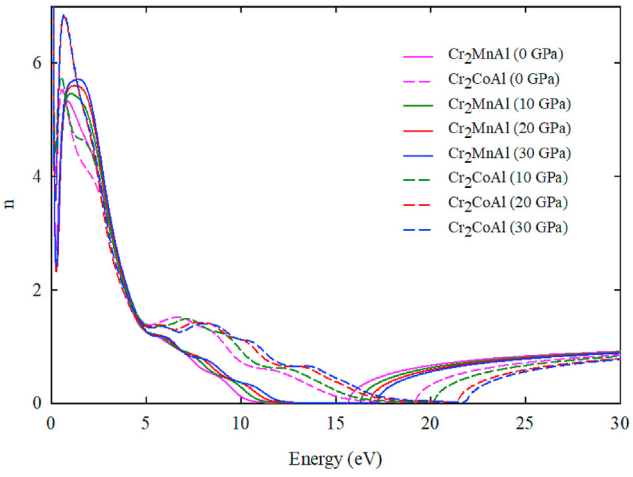

Figure 10. Static refractive index of Cr_2MnAl and Cr_2CoAl at pressures from 0 to 30 GPa at an interval of 10 GPa.

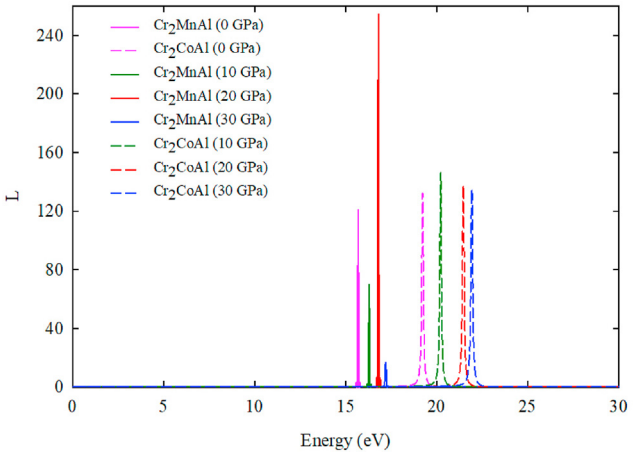

Figure 12. Loss function of Cr_2MnAl and Cr_2CoAl at pressures from 0 to 30 GPa at an interval of 10 GPa.

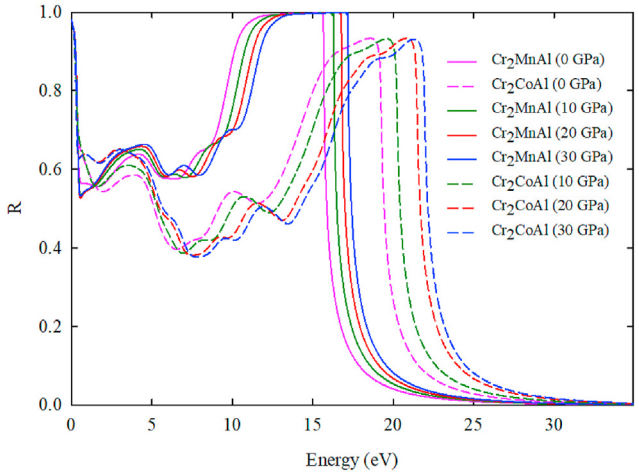

Figure 13. Reflectivity of Cr_2MnAl and Cr_2CoAl at pressures from 0 to 30 GPa at an interval of 10 GPa.

Figure 12 shows the variation of the loss function (L) of Cr_2CoAl and Cr_2MnAl with incident photon energy at various external pressures up to 30 GPa. The sharp peak located at 19 eV (16 eV) corresponds to the bulk screened plasma frequency, ω_p for Cr_2CoAl (Cr_2MnAl). The peaks shift towards higher photon energies in both compounds as the external pressure increases up to 30 GPa.

From the reflectivity spectrum of the compounds at pressures up to 30 GPa at an interval of 10 GPa (Figure 13), the high value of reflectivity, $R(\omega)$ is observed in the energy range 0–18 eV at 0 GPa. This property may present Cr_2MnAl and Cr_2CoAl as potential candidates to construct opto-electronic devices. A sharp decrease in the reflectivity at 0 GPa from high value is evident from Figure 13 at about 16 eV and 19 eV for Cr_2MnAl and Cr_2CoAl, respectively, which is consistent with the loss function spectrum as shown in Figure 12. The photon energy at which the sharp decrease in the reflectivity is observed shifts towards the higher photon energy with increasing external pressure. The effect of pressure on R seems similar for both compounds.

Another indication of the metallic nature of the material Cr_2CoAl is obtained from the finite value of the photoconductivity at very small incident energy (Figure 14). Photoconductivity of both the Heusler compounds Cr_2CoAl and Cr_2MnAl increases gradually in the visible range of the electromagnetic spectrum from zero photon energy and reaches maximum at about 3 eV. Maximum photoconductivity of Cr_2MnAl is higher than that of Cr_2CoAl. The peak height at 3 eV for both the compounds increases with external pressure over the studied pressure range.

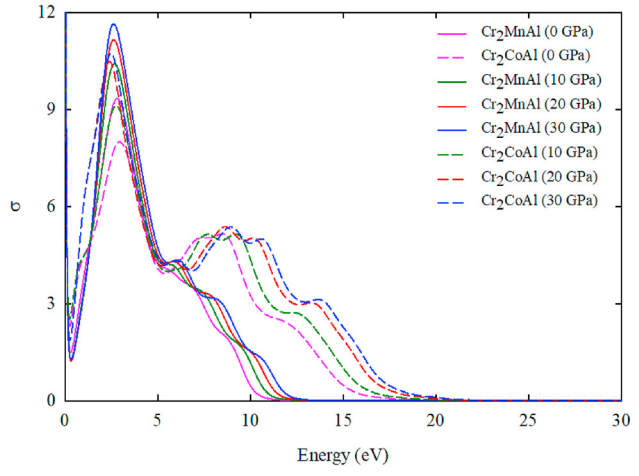

Figure 14. Photoconductivity of Cr_2CoAl of Cr_2MnAl at pressures from 0 to 30 GPa at an interval of 10 GPa.

4. Conclusion

DFT based calculations are carried out on the study of hydrostatic pressure effect (up to 30 GPa) on the structural, elastic, mechanical, electronic and optical properties of the Heusler compounds Cr_2MnAl and Cr_2CoAl. Calculated ground state lattice constants of these compounds agree well with previous experimental and computational studies. The progressive decrease of lattice parameters and unit cell volume with pressure is an indication of structural stability of the studied compounds at elevated pressure up to 30 GPa. The absence of the imaginary frequency in our calculated phonon dispersion curves reveals the dynamical stability of these compounds at elevated pressure up to 30 GPa. The increase of elastic constants with pressure reveals the mechanical stability of these compounds in the considered pressure range. The calculated limiting values of Pugh's ratio, Poisson's ratio and Cauchy pressure indicates the brittleness of Cr_2MnAl while those indicate the ductility of Cr_2CoAl. The gradual increase of Debye temperature with hydrostatic pressure points out the rigidity of both compounds at elevated pressure. Investigations of electronic band structure and DOS at 0 GPa reveals that the spin polarization for Cr_2MnAl is 100%, i.e., DOS at E_F is zero for one of the spin channels and non-zero for other spin channel. Our electronic structure calculations show that the Heusler compound Cr_2MnAl is a half-metal and Cr_2CoAl is a near half-metal. The pressure dependent electronic structure calculations show that the near half metallicity of Cr_2CoAl and the half metallicity of Cr_2MnAl disappear at ~30 GPa. The optical properties of these compounds are investigated by applying the polarized electromagnetic radiation. Reflectivity and absorption spectrum are very much consistent with the dependence of the dielectric function with incident photon energy for both Cr_2MnAl and Cr_2CoAl. High value of reflectivity of these compounds make them promising in the industrial applications for optoelectronic devices. Metallic behaviour of these compounds is also confirmed from the absorption spectrum.

Declarations

Author contribution statement

M. Jubair: Conceived and designed the experiments; Performed the experiments; Analyzed and interpreted the data; Wrote the paper.

A. M. M. Tanveer Karim, M. Nuruzzaman, M. A. K. Zilani: Conceived and designed the experiments; Analyzed and interpreted the data; Wrote the paper.

M. Roknuzzaman: Performed the experiments; Analyzed and interpreted the data.

Funding statement

This research did not receive any specific grant from funding agencies in the public, commercial, or not-for-profit sectors.

Data availability statement

Data will be made available on request.

Declaration of interests statement

The authors declare no conflict of interest.

Additional information

No additional information is available for this paper.

References

[1] T. Graf, C. Felser, S.S.P. Parkin, Simple rules for the understanding of Heusler compounds, Prog. Solid State Chem. 39 (2011) 1–50.

[2] J.M. Shaw, E.K. Delczeg-Czirjak, E.R.J. Edwards, Y. Kvashnin, D. Thonig, M.A.W. Schoen, M. Pufall, M.L. Schneider, T.J. Silva, O. Karis, K.P. Rice, O. Eriksson, H.T. Nembach, Magnetic damping in sputter-deposited Co_2MnGe Heusler compounds with A2,B2 , and $L2_1$ orders: experiment and theory, Phys. Rev. B 97 (2018) 94420.

[3] H. Lin, L.A. Wray, Y. Xia, S. Xu, S. Jia, R.J. Cava, A. Bansil, M.Z. Hasan, Half-Heusler ternary compounds as new multifunctional experimental platforms for topological quantum phenomena, Nat. Mater. 9 (2010) 546–549.

[4] S. Tsunegi, Y. Sakuraba, M. Oogane, H. Naganuma, K. Takanashi, Y. Ando, Enhancement in tunnel magnetoresistance effect by inserting CoFeB to the tunneling barrier interface in Co_2MnSi/MgO/CoFe magnetic tunnel junctions, Appl. Phys. Lett. 94 (2009) 252503.

[5] J. Ma, J. He, D. Mazumdar, K. Munira, S. Keshavarz, T. Lovorn, C. Wolverton, A.W. Ghosh, W.H. Butler, Computational investigation of inverse Heusler compounds for spintronics applications, Phys. Rev. B 98 (2018) 94410.

[6] T. Sebastian, Y. Ohdaira, T. Kubota, P. Pirro, T. Brächer, K. Vogt, A.A. Serga, H. Naganuma, M. Oogane, Y. Ando, B. Hillebrands, Low-damping spin-wave propagation in a micro-structured $Co_2Mn_{0.6}Fe_{0.4}Si$ Heusler waveguide, Appl. Phys. Lett. 100 (2012) 112402.

[7] T. Seki, H. Yako, T. Yamamoto, T. Kubota, Y. Sakuraba, M. Ueda, K. Takanashi, Spin torque-induced magnetization dynamics in giant magnetoresistance devices with Heusler alloy layers, J. Phys. D Appl. Phys. 48 (2015) 164010.

[8] T. Yamamoto, T. Seki, K. Takanashi, Vortex spin-torque oscillator using $Co_2Fe_xMn_{1-x}Si$ Heusler alloys, Phys. Rev. B 94 (2016) 94419.

[9] S. Mizukami, F. Wu, A. Sakuma, J. Walowski, D. Watanabe, T. Kubota, X. Zhang, H. Naganuma, M. Oogane, Y. Ando, T. Miyazaki, Long-lived ultrafast spin precession in manganese alloys films with a large perpendicular magnetic anisotropy, Phys. Rev. Lett. 106 (2011) 117201.

[10] D. Xiao, Y. Yao, W. Feng, J. Wen, W. Zhu, X.-Q. Chen, G.M. Stocks, Z. Zhang, Half-heusler compounds as a new class of three-dimensional topological insulators, Phys. Rev. Lett. 105 (2010) 96404.

[11] M. Meinert, Unconventional superconductivity in YPtBi and related topological semimetals, Phys. Rev. Lett. 116 (2016) 137001.

[12] O. Pavlosiuk, D. Kaczorowski, P. Wiśniewski, Superconductivity and Shubnikov–de Haas oscillations in the noncentrosymmetric half-Heusler compound YPtBi, Phys. Rev. B 94 (2016) 35130.

[13] C. Chen, A first-principles study of a new Heusler alloy, Int. J. Mater. Sci. Appl. 6 (2017) 108.

[14] M.E. Jamer, L.G. Marshall, G.E. Sterbinsky, L.H. Lewis, D. Heiman, Low-moment ferrimagnetic phase of the Heusler compound Cr_2CoAl, J. Magn. Magn. Mater. 394 (2015) 32–36.

[15] A. Datta, M. Modak, M. Kundu, S. Banerjee, Negative magnetization in inverse Heusler alloy Cr2CoAl, in: DAE Solid State Physics Symposium 2018, 2019.

[16] A. Nagpal, B. Agrawal, R. Kumar, H.S. Saini, M.K. Kashyap, M. Singh, Effect of Disorders on Half-Metallic Ferromagnetism in Cr_2CoAl Inverse Heusler alloy, 2019.

[17] J. Li, Y. Li, G. Zhou, Y. Sun, C.Q. Sun, A first principles study on the full-Heusler compound Cr_2MnAl Appl, Phys. Lett. 94 (2009) 242502.

[18] H. Rached, D. Rached, R. Khenata, B. Abidri, M. Rabah, N. Benkhettou, S.B. Omran, A first principle study of phase stability, electronic structure and magnetic properties for $Co_{2-x}Cr_xMnAl$ Heusler alloys, J. Magn. Magn. Mater. 379 (2015) 84–89.

[19] M. Rasheduzzaman, K.M. Hossain, S.K. Mitro, M.A. Hadi, J.K. Modak, M.Z. Hasan, Structural, mechanical, thermal, and optical properties of inverse-Heusler alloys Cr_2CoZ (Z = Al, In): a first-principles investigation, Phys. Lett. A 385 (2021) 126967.

[20] M. Singh, H.S. Saini, J. Thakur, A.H. Reshak, M.K. Kashyap, Tuning Fermi level of Cr_2CoZ (Z=Al and Si) inverse Heusler alloys via Fe-doping for maximum spin polarization, J. Magn. Magn. Mater. 370 (2014) 81–86.

[21] H.S. Jin, K.W. Lee, Stability of room temperature compensated half-metallicity in Cr-based Inverse-Heusler Compounds, Curr. Appl. Phys. 19 (2019) 193–197.

[22] S. Qi, C.H. Zhang, B. Chen, J. Shen, First-principles study on the band structure, magnetic and elastic properties of half-metallic Cr_2MnAl Mod, Phys. Lett. B 29 (2015) 1550139.

[23] S.J. Clark, M.D. Segall, C.J. Pickard, P.J. Hasnip, M.I.J. Probert, K. Refson, M.C. Payne, First principles methods using, CASTEP Z. Kristallogr. - Cryst. Mater. 220 (2005) 567–570.

[24] P. Hohenberg, W. Kohn, Inhomogeneous, Electr. Gas Phys. Rev. 136 (1964) B864–B871.

[25] W. Kohn, L.J. Sham, Self-consistent equations including exchange and correlation effects, Phys. Rev. 140 (1965) A1133–A1138.

[26] J.P. Perdew, K. Burke, M. Ernzerhof, Generalized gradient approximation made simple, Phys. Rev. Lett. 77 (1996) 3865–3868.

[27] D. Vanderbilt, Soft self-consistent pseudopotentials in a generalized eigenvalue formalism, Phys. Rev. B 41 (1990) 7892–7895.

[28] T.H. Fischer, J. Almlof General methods for geometry and wave function optimization, J. Phys. Chem. 96 (1992) 9768–9774.

[29] H.J. Monkhorst, J.D. Pack, Special points for Brillouin-zone integrations, Phys. Rev. B 13 (1976) 5188–5192.

[30] K. Refson, P.R. Tulip, S.J. Clark, Variational density-functional perturbation theory for dielectrics and lattice dynamics, Phys. Rev. B 73 (2006) 155114.

[31] F.D. Murnaghan, Finite deformation of an elastic solid, Amer. Math. Soc. 59 (1951) 235.

[32] M. Jamal, S.J. Asadabadi, I. Ahmad, H.A.R. Aliabad, Elastic constants of cubic crystals Comput, Mater. Sci. 95 (2014) 592–599.

[33] F. Mouhat, F.X. Coudert, Necessary and sufficient elastic stability conditions in various crystal systems, Phys. Rev. B 90 (2014) 224104.

[34] J. Wang, S. Yip, S.R. Phillpot, D. Wolf, Crystal instabilities at finite strain, Phys. Rev. Lett. 71 (1993) 4182–4185.

[35] R. Hill, The elastic behaviour of a crystalline aggregate, Proc. Phys. Soc. Lond. Sect. A 65 (1952) 349–354.

[36] W. Voigt, Lehrbuch der kristallphysik (mit ausschluss der kristalloptik), in: bg teubner, jw edwards (Eds.), leipzig berlin, 1928. Ann Arbor, Mich.

[37] A. Yildirim, H. Koc, E. Deligoz, First-principles study of the structural, elastic, electronic, optical, and vibrational properties of intermetallic Pd_2Ga Chin, Phys. B 21 (2012) 37101.

[38] C. Kittel, Introduction to Solid State Physics Eighth Editions, Library of Congress Cataloging, 2005.

[39] S.F. Pugh XCII, Relations between the elastic moduli and the plastic properties of polycrystalline pure metals, Lond. Edinb. Dublin Phil. Magaz. J. Sci. 45 (1954) 823–843.

[40] G.N. Greaves, A.L. Greer, R.S. Lakes, T. Rouxel, Poisson's ratio and modern materials, Nat. Mater. 10 (2011) 823–837.

[41] W. Feng, S. Cui, Mechanical and electronic properties of Ti_2AlN and Ti_4AlN_3: a first-principles study Can, J. Phys. 92 (2014) 1652–1657.

[42] L. Kleinman, Deformation potentials in silicon. I. Uniaxial strain, Phys. Rev. 128 (1962) 2614–2621.

[43] M. Mattesini, R. Ahuja, B. Johansson Cubic Hf_3N_4 and Zr_3N_4: a class of hard materials, Phys. Rev. B 68 (2003) 184108.

[44] Y. Han, Y. Wu, T. Li, R. Khenata, T. Yang, X. Wang, Electronic, magnetic, half-metallic, and mechanical properties of a new equiatomic quaternary Heusler compound YRhTiGe, A First-Prin. Study Mater. 11 (2018) 797.

[45] O.L. Anderson, A simplified method for calculating the Debye temperature from elastic constants, J. Phys. Chem. Solid. 24 (1963) 909–917.

[46] A. Pasturel, C. Colinet, P. Hicter, Strong chemical interactions in disordered alloys, Phys. B+C 132 (1985) 177–180.

[47] Z.Q. Lv, W.T. Fu, S.H. Sun, Z.H. Wang, W. Fan, M.G. Qv, Structural, electronic and magnetic properties of cementite-type Fe3X (X=B, C, N) by first-principles calculations, Solid State Sci. 12 (2010) 404.

[48] R. Saniz, L.H. Ye, T. Shishidou, A.J. Freeman, Structural, electronic, and optical properties of $NiAl_3$: first-principles calculations, Phys. Rev. B 74 (2006) 14209.

[49] CASTEP User Guide from Materials Studio. http://www.castep.org/CASTEP/Documentation.

[50] F.A. Modine, R.W. Major, T.W. Haywood, G.R. Gruzalski, D.Y. Smith, Optical properties of tantalum carbide from the infrared to the near ultraviolet, Phys. Rev. B 29 (1984) 836–841.